

Internal Structure in virialized halos of dark matter

© E.V. Mikheeva^{1,2}, A.G Doroshkevich^{1,3}, V.N. Lukash^{1,4},

¹ Astro Space Centre of P.N. Lebedev Physics Institute of RAS, Moscow, Russia

² Email: helen@asc.rssi.ru

³ Email: dorr@asc.rssi.ru

⁴ Email: lukash@asc.rssi.ru

Abstract: We propose a solution of the cusp problem in framework of the standard Λ CDM cosmology. To provide this we describe the linear and nonlinear periods of halo formation by the entropy function of dark matter particles. This approach allows us to take into account together the impacts of both the small scale initial velocity perturbations in collapsed halos and the processes of nonlinear relaxation of compressed matter. We show that these small scale random velocities suppress the formation of cusp-like halos and favor the creation of core-like ones. This approach allows us to reproduce observed rotation curves, to explain their random scatters and deviations from simulated ones.

1. Introduction

The cusp problem is one of the most intriguing widely discussed during last years. It comes from numerical simulations always predicting the formation of divergent density profiles in inner parts of simulated virialized dark matter objects (halos). However, observational picture is different, sometime cusp-like density profiles can be seen indeed, but much more often we register more smother behavior of density profiles in the inner part of galaxies. This contradiction is known as "the cusp problem".

Mathematically, this means that assuming in the central part of gravitationally-bounded halos the power-law density profile

$$\rho(r) \propto r^{-\alpha}, \quad (1)$$

we get $\alpha \geq 1$ in numerical simulations (e.g. [1]) and $\alpha < 1$ in real galaxies (e.g. [2-4]). So, in the first case we deal with cusp-like behavior of density profile, in the second one with core-like behavior. Available observational data demonstrate a broad scatter of α (see [2-4]) and sometimes $\alpha > 1$ are observed, mainly in rich clusters of galaxies [5]). In addition, a majority of the observed rotation curves of galaxies [6] are well fitted by the Burkert's function with $\alpha = 0$ (see [7]) which differs significantly from the simulated curves fitted by the Navarro-Frenk-White (NFW) function with $\alpha = 1$ ([8-10]).

This situation has created the problem discussed during many years as an important problem of the standard Λ CDM cosmology. More of that, there is a common myth that the relaxation of collisionless dark matter particles always produces cusps in density profiles.

2. Physical nature of difference between cusp and core

To clarify the difference between core and cusp we calculate pressure profile for gravitationally-bounded dark matter halo. For power-law density profile (1) we get for the mass of halo

$$M = M(r) = \int_0^r \rho(r) r^2 dr \propto r^{3-\alpha}.$$

Assuming hydrostatical equilibrium within a halo

$$\frac{1}{\rho(r)} \frac{dp(r)}{dr} = - \frac{GM(r)}{r^2} \propto r^{1-\alpha},$$

where $p(r)$ is a pressure of dark matter particles, we conclude

$$p(r) = C_1 + C_2 r^{2(1-\alpha)},$$

where C_1 and C_2 are some constants. So, if $\alpha \leq 1$ then the pressure in the central part of halo is finite and we have the core. If $\alpha > 1$ then the pressure is infinite what corresponds to the cusp. Evidently, $\alpha = 1$ is a critical value of α .

The halo formation includes both processes of the reversible matter compression and the irreversible relaxation. To discriminate between them we consider the entropy function, $F(r)$. For the nonrelativistic dark matter particles with the isotropic pressure the entropy function can be written as follows:

$$p(r) = \rho \langle v^2 \rangle = nT = F(r)n(r)^{5/3},$$

where v is one-dimensional random velocity, ρ , n and T are the density, concentration and temperature of dark matter particles. Here F is presented as a function of current radius of halo, r , but it is more convenient to consider it as a function of current mass, i.e. mass inside of r . We call $F(M)$ by entropy mass function:

$$F(M) \propto C_1 M^{\beta_1} + C_2 M^{\beta_2} \propto M^\beta,$$

where

$$\beta_1 = \frac{5\alpha}{3(3-\alpha)}, \quad \beta_2 = \frac{6-\alpha}{3(3-\alpha)}, \quad \beta \in (\beta_1, \beta_2). \quad (2)$$

The critical value $\alpha_{cr} = 1$ corresponds to the critical value $\beta_{cr} = \beta_1 = \beta_2 = 5/6$.

The entropy mass function integrates the impact of irreversible processes during the whole evolution of dark matter and determines the profile of relaxed dark matter halo. As is seen from (2) for $\alpha < 3$ we have $\beta_1 \geq 0$, $\beta_2 \geq 0$ and, so, $F(M) \rightarrow 0$ for $M \rightarrow 0$. However, the fraction of low entropy dark matter particles in the central regions of halo in the cusp case is larger than that in the case of core (see Figure 1).

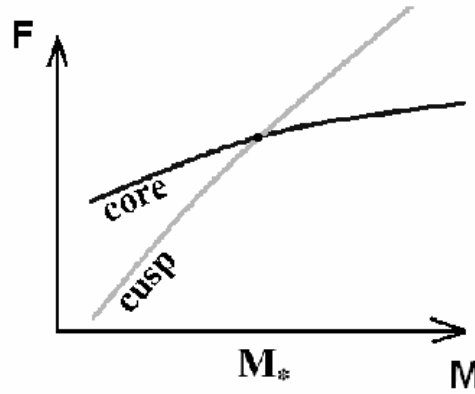


Fig.1 Entropy mass functions $F(M)$ versus the current mass in cases of core and cusp in density profile of gravitationally bounded halo of dark matter.

3. Idea and method

The discussions of the halo formation are usually concentrated around the processes of dark matter relaxation which are main sources of entropy. At the same time it is usually accepted that before matter relaxation the dark matter entropy is negligible. However, in the CDM model there are random correlated velocities down to very small scales determined by the mass of dark matter particles. In a course of the matter compression they are partly transformed to the temperature of particles and, so, increase the entropy mass function at small M . This effect can be estimated analytically. Further on we calculate the joint entropy in relaxed dark matter halos summing the initial entropy given by small scale initial perturbations and the entropy generated during non-linear relaxation of collapsed matter.

Our further analysis includes the following steps:

1. Instead of density-radius relation we use the entropy-mass profile.
2. The mean initial (background) entropy profile, $F_b(M)$, is estimated as the entropy mass function of linear velocity perturbations. Such identification assumes the almost adiabatic matter compression and, so, partly underestimates the entropy mass function $F_b(M)$ at small M .
3. The entropy generated by the process of relaxation of compressed matter, $F_g(M)$, is taken from results of N-body simulations (e.g. NFW profile).
4. We combine the initial and generated entropies by a simple way to set of joint entropy profiles and reconstruct the circular velocities and resulting density profiles.

4. Initial entropy mass function

At the beginning we need to consider initial field of density perturbations and its statistical properties.

Let us characterize the initial conditions in dark matter by three gauge-invariant variables — displacement of a matter point from unperturbed position (the deviation from Hubble flows), $\vec{S}(\vec{x})$, the full velocity of matter, $\vec{V}(z, \vec{x})$, and comoving density perturbation, $\delta(z, \vec{x}) \equiv \rho(z, \vec{x}) / \rho(z) - 1$:

$$\vec{r}(z, \vec{x}) = \frac{1}{1+z} [\vec{x} - g(z)\vec{S}(\vec{x})], \quad \vec{V}(z, \vec{x}) = \dot{\vec{r}} = H(\vec{r} + g(z)\vec{S}(\vec{x})),$$

$$\delta(z, \vec{x}) = g(z) \cdot \delta(\vec{x}), \quad \delta(\vec{x}) = \text{div } \vec{S} = \partial S_i / \partial x_i,$$

where the dot and prime mean derivative with respect to the physical time and the function argument, $\vec{r}(z, \vec{x})$ and \vec{x} are the Eulerian (shear-free) and Lagrangian (comoving) coordinates of a matter point.

In these terms perturbations related with the collapsed halo as whole and conditional perturbations within the halo can be separated as follows:

$$\vec{S}(\vec{x}) = \vec{S}_R(\vec{x}) + \vec{S}_*(\vec{x}),$$

$$\delta(\vec{x}) = \delta_R(\vec{x}) + \delta_*(\vec{x}),$$

where quantities with index R are related to a protohalo with a linear size R , and quantities with index $*$ corresponds to conditional perturbations which determine the temperature and entropy of compressed matter,

$$\langle \vec{S}_* \rangle = \langle \delta_* \rangle = 0,$$

$$\langle \vec{S}_*^2 \rangle \equiv \sigma(R)_*^2 = \int P(k) [1 - W(kR)]^2 dk,$$

where $W(x)$ is a spherical window function.

After analytical and numerical calculations we obtain the values of the power index β of initial entropy mass function $F(M)$ as a function of the current mass, $M \leq 10^n M_\odot$. β for some important values of the mass are listed in the Table 1.

Table 1 Power index of the function $F \propto M^\beta$ for halos with $M \leq 10^n M_\odot$..

$n \equiv \log(M / M_\odot)$	10	7	5	≤ 5
$\beta \equiv d \ln F(M) / d \ln M$	0.3	0.5	0.57	0.67

It is easy to see that in all cases β is less than the critical value $\beta_{cr} = 5/6$. This means that the initial entropy dominates in the central regions of halo what stimulates the formation of cores and suppresses the cusp formation.

5. Entropy generation during the matter relaxation

The spherical collapse with the violent relaxation of compressed matter has been investigated in many papers. Thus, authors of [11] started from initial conditions with no initial velocities and entropy

$$\delta M(r) = 1 - M(r) / \langle M(r) \rangle \propto \langle M(r) \rangle^{-\varepsilon},$$

$$v_i = 0,$$

$$\delta \rho = \rho_{in}(r) - \langle \rho_{in} \rangle \propto r^{-3\varepsilon},$$

$$\langle M(r) \rangle \propto r^3,$$

and found that the density profile of relaxed matter, $\rho(r)$, is approximated at small r by power law:

$$\rho(r) \propto r^{-\alpha},$$

$$\alpha = 2, \text{ for } \varepsilon \leq 2/3$$

$$\alpha = 9\varepsilon / (1 + 3\varepsilon), \text{ for } \varepsilon \geq 2/3 \quad (3)$$

The approach was extended in [12, 13] where non-radial trajectories of dark matter particles were also considered. The density profiles for relaxed halos were found to be similar to the previous one.

This problem have also been considered in [14, 15] for the initial conditions

$$v(r) = 0,$$

$$\rho(x) = \rho_0 \left(1 - r^2 / r_0^2\right).$$

Near the center of cloud the power law density profile was found with

$$\rho(r) \propto r^{-\alpha}, \quad \alpha \approx 1.7 - 1.9.$$

Anywhere initial velocities and entropy was accepted to be equal to zero.

As it is seen from these relations, the model of *violent relaxation* leads to the entropy distribution

$$M(r) \propto r,$$

$$F_g(r) \propto r^{4/3} \propto M^{4/3}, \quad \beta = 4/3 \geq \beta_{cr},$$

that implies the formation of cusp. However, in the central regions of halos the entropy generated by this process becomes negligible as compared with the initial entropy. Thus, the influence of the former restricts the central density of halos and prevents formation of cusp-like density profile.

The same conclusion is valid also for the simulated NFW – density profile with $\alpha = \alpha_{cr} = 1$,

$\beta = \beta_{cr} = 5/6$ which represents the more general model of *hierarchical* halo formation. The drop of these indices as compared with previous ones indicates that in the case the initial entropy is partly allowed for but owing to the small scale cutoff of the simulated power spectra its impact is underestimated as compared with estimates in the Table 1..

6. Rotation curves caused by the joint entropy

The shape of rotation curves is determined by sum of initial and generated entropy. To clarify their influence we model the joint entropy mass function as follows:

$$F(M) = \sqrt{F_b^2 + F_g^2}, \quad F_b \equiv \kappa F.$$

where the factor, κ ($0 \leq \kappa \leq 1$), measures the relative contribution of the initial entropy within a characteristic mass for different halos.

Now we can calculate rotation curves and compare them with observed and simulated ones. The results are presented in Fig 2, where the circular velocities, v_c , are plotted versus radius for six models of hierarchical ($\beta_g = 5/6$, left plot) and six models of violent ($\beta_g = 4/3$, right plot) relaxation processes for initial conditions with $\beta_b = 0.333, 0.567, 0.667$ and for $\kappa \ll 1$ and $\kappa \gg 1$. Both the velocities and radius are normalized for their values in point of velocity maximum, $v_{max} = v_c(r_{max}) \geq v_c(r)$. The curves are compared with the NFW and Burkert ones.

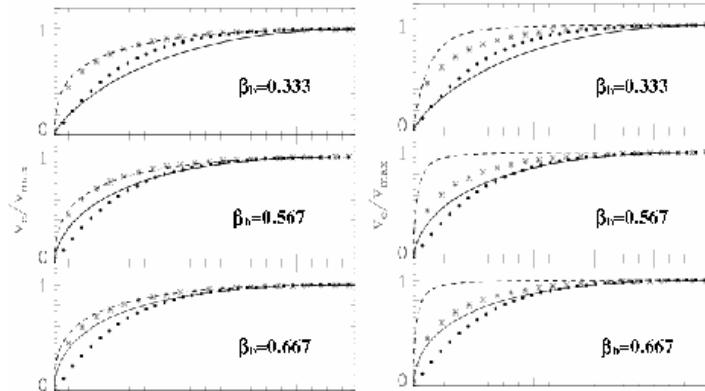


Fig.2 Normalized rotation curves are plotted for the models of hierarchical (left side of the Figure) and violent (right side) relaxation for $\kappa_s \ll 1$ and $\kappa_s \approx 1$ (dashed and solid lines). NFW and Burkert fits are plotted by stars and dots, respectively.

As is seen from this Figure, the rotation curves for our models with $\beta = 1/3$ and $0 \leq \kappa_s \leq 1$ close the gap between the Burkert and NFW rotation curves. So, we can expect that properties of observed curves can be successfully reproduced by our models with suitable values of κ and β_b . The scatter of both initial and generated entropies can provides required variations of these parameters and the shape of rotation curves what, in turn, explains variations of observed rotation curves.

Let us note also that for low mass halos with $\beta_b = 0.567$ and especially $\beta_b = 2/3$ all rotation curves with $0 \leq \kappa \leq 1$ are concentrated nearby the NFW profile. This fact indicates that for dwarf galaxies with

$M \leq 10^8 M_{\odot}$ the observed rotation curves can be similar to expected ones for the model of hierarchical clustering with the NFW profile.

7. Conclusions

We conclude, that

1. The initial entropy can prevent the cusp formation for halos with dark matter masses $10^8 - 10^{12} M_{\odot}$. For smaller and larger galaxies and for clusters of galaxies the impact of the initial entropy is attenuated.
2. The impact of the initial entropy allows to reproduce the observed rotation curves and many helps to solve the so called "cusp problem".

Acknowledgments.

This work was supported by Russian Foundation for Basic Research (grant numbers 07-02-00886 and 08-02-00159).

Conclusions

1. Diemand J., Moore B., Stadel J. // *Nature* 433, 389 (2005).
2. de Blok W.J.G., McGaugh S.S., Bosma A., Rubin V. // *ApJ* 552, L23 (2001).
3. Swaters R.A., Madore B.F., van den Bosch F.C., Barcella M. // *ApJ* 583, 732 (2003).
4. Swaters R.A., Madore B.F., van den Bosch F.C., Barcella M. // *ApJ* 576, L19 (2003).
5. Pointecouteau E., Arnaud M., Pratt G.W. // *A&A* 435, 1 (2005).
6. Marchezini D. et al. // *ApJ* 575, 801 (2002).
7. Buerkert A. // *ApJ* 447, L25 (1995).
8. Navarro J.F., Frenk C.S., White S.D.M. // *MNRAS* 275, 720 (1995).
9. Navarro J.F., Frenk C.S., White S.D.M. // *ApJ* 462, 563 (1996).
10. Navarro J.F., Frenk C.S., White S.D.M. // *ApJ* 490, 1666 (1997).
11. Fillmore J.A., Goldreich P. // *ApJ* 281, 1 (1984).
12. Sikivie P., Tkachev I.I., Wang Yun // *Phys.Rev D* 56, 1863 (1997).
13. Nusser A. // *MNRAS* 325, 1397 (2001).
14. Gurevich A.V. Zybin K.P. // *ZHETF* 94, 5 (1988).
15. Gurevich A.V., Zybin K.P. // *Physics-Uspokhi* 38, 687 (1995).